INORGANIC CHEMISTRY
FRONTIERS

RESEARCH ARTICLE

View Article Online
View Journal | View Issue

Check for updates

Cite this: *Inorg. Chem. Front.*, 2024, **11**, 5905

Multi-step cation substitution facilitating the exploration of potential infrared nonlinear optical materials†

Ya-Xiang Han,[a,b] Chun-Li Hu,[a] Wen-Tong Chen[c] and Jiang-Gao Mao *[a]

Crystal structure regulation and optical performance enhancement are huge challenges, especially for the laborious and inefficient trial-and-error method, in the research on infrared nonlinear optical (IR NLO) materials. In this work, multi-step cation substitutions were adopted to modulate the crystal structure for the effective design of well-performing IR NLO materials. Specifically, starting from the famous $AgGaS_2$ (AGS, $I\bar{4}2d$) crystal, Ag_2CdSiS_4 ($Pmn2_1$) with diamond-like crystal structure, $BaAg_2SiS_4$ ($I\bar{4}2m$) with three-dimensional tunnel structure and $LaAgSiS_4$ ($Ama2$) with two-dimensional layer structure were designed and experimentally synthesized through multi-step cation substitutions. Structural analysis reveals the fundamental reason of their tetrahedral framework transformation: the size effect of cations and the reduction of component tetrahedra caused by cationic substitution change the assembly mode of the tetrahedral units. Additionally, three non-centrosymmetric Ag-based thiosilicates exhibit wide transmittance range (0.5–17 μm), higher laser-induced damage thresholds (2 times that of AGS) and significant phase-matchable second harmonic generation (SHG) enhancement from 0.6 to 3.2 times that of AGS. This work demonstrates that multi-step cation substitution is an effective way to extend non-centrosymmetric structures, which facilitate the exploration of potential infrared nonlinear optical materials.

Received 26th June 2024,
Accepted 28th July 2024

DOI: 10.1039/d4qi01603c

rsc.li/frontiers-inorganic

Open Access Article. Published on 29 2024. Downloaded on 2025/11/30 15:27:48.
This article is licensed under a Creative Commons Attribution-NonCommercial 3.0 Unported Licence.

Introduction

With the advancement of optical fields such as optical communication, optical imaging, laser guidance, and environmental monitoring,[1–4] there is a growing demand for infrared nonlinear optical (IR NLO) crystals with exceptional properties including large second harmonic generation (SHG) response, phase matching capabilities (suitable Δn), high laser-induced damage threshold (LIDT), wide light transmission range, and good physical and chemical stability.[5] Prominent commercially available IR NLO materials include chalcopyrite-type ionic crystals $AgGaS_2$ (AGS), $AgGaSe_2$ (AGSe), and $ZnGeP_2$ (ZGP), which are known for their large second harmonic generation (SHG) responses and broad IR transparency. However, their potential applications are significantly constrained by inherent limitations, including a low laser induced damage threshold (LIDT), poor phase matching ability and harmful two-photon absorption.[6–8]

Great efforts have been devoted to the exploration of new IR SHG materials.[9–12] A series of tetrahedron-based compounds, such as $AgGa_2PS_6$ (1 × AGS), $Hg_3P_2S_8$ (4.2 × AGS) and $Li_4MgGe_2S_7$ (0.7 × AGS), were produced by combinations between different tetrahedral active groups.[13–16] Choosing $[AsS_3]^{3-}$ and $[SbS_3]^{3-}$ anions with stereochemical lone pair electrons or π-conjugated planar triangular $[BS_3]^{3-}$ as infrared nonlinear optical genes led to the isolation of new IR SHG crystals such as $LaBS_3$ (1.2 × AGS) and $BaHgSe_2$ (1.5 × AGS).[17–20] Alkaline-earth or transition metal cations were introduced to adjust the band gaps as in $BaGa_4S_7$ (0.9 × AGS) and Cd_4SiS_6 (1.3 × AGS).[21–26] Searching for new IR NLO material systems, such as pnictides, oxyhalides and adducts, led to the discovery of new materials such as $RuSi_4P_4$ (1.4 × AGS), $Pb_{17}O_8Cl_{18}$ (2 × AGS), $Pb_{18}O_8Cl_{15}I_5$ (1 × AGS) and $(CuBr)_7(P_4Se_3)_3$ (3.5 × AGS).[27–31]

Despite great achievements, most previous explorations are based on the laborious and inefficient trial-and-error synthetic

[a]*State Key Laboratory of Structural Chemistry, Fujian Institute of Research on the Structure of Matter, Chinese Academy of Sciences, Fuzhou, 350002, P. R. China. E-mail: mjg@fjirsm.ac.cn*
[b]*University of Chinese Academy of Sciences, Beijing 100039, P. R. China*
[c]*Institute of Applied Chemistry, School of Chemistry and Chemical Engineering, Ji'an Key Laboratory of Photoelectric Crystal Materials and Device, Jiangxi Province Key Laboratory of Coordination Chemistry, Humic Acid Utilization Engineering Research Center of Jiangxi Province, Jinggangshan University, Ji'an, Jiangxi 343009, China*

†Electronic supplementary information (ESI) available: Syntheses, methods, instrumentations, computational details, crystallographic data, dipole moments, LIDT test, powder XRD, EDS, IR and UV–vis–NIR spectra, and computational results of title compounds. CCDC 2343723, 2343733 and 2343740. For ESI and crystallographic data in CIF or other electronic format see DOI: https://doi.org/10.1039/d4qi01603c

Open Access Article. Published on 29 2024. Downloaded on 2025/11/30 15:27:48.
This article is licensed under a Creative Commons Attribution-NonCommercial 3.0 Unported Licence.

methods.[32] Researchers are starting to find more efficient ways to design new IR NLO materials. One good way is based on computer-assisted structure and optical property prediction, which led to the discovery of $Zn_3(PS_4)_2$ (52 × KH_2PO_4), Zn_2BS_3Br (2 × AGS), *etc.*[33–35] Another strategy is to screen potential nonlinear optical materials, such as $LiGaSe_2$ (2 × AGS), from the database.[36] In addition, chemical substitutions were also considered an effective way to explore novel nonlinear optical crystals. For example, $BiFSeO_3$ with strong SHG response of 13.5 times than that of $KH_2(PO)_4$ at 1064 nm was obtained using $[SeO_3]^{2-}$ and F^- to simultaneously aliovalently substitute the $[IO_3]^-$ and O^{2-} anions.[37] However, in previous reports, such works have only involved single-step substitution and similar crystal structures. Related systematic studies on structure and performance regulation are scarce, prompting us to utilize multi-step cation substitutions to extend more crystal structure types.[38,39]

To experimentally prove the effectiveness of multi-step cation substitution, the famous AGS was selected as the template due to its dominant diamond-like structure.[40–44] First, Ag_2CdSiS_4 with a similar diamond-like structure was designed using one Cd^{2+} and one Si^{4+} to substitute two Ga^{3+} in AGS. Second, to preliminarily break the tetrahedral close-packed framework, Ba^{2+} with larger radius was adopted to substitute Cd^{2+} in Ag_2CdSiS_4, producing the three-dimensional tunnel structural $BaAg_2SiS_4$. Finally, by substituting one Ba^{2+} and one Ag^+ with a La^{3+}, $LaAgSiS_4$ was created, forming two-dimensional $[AgSiS_4]^{3-}$ layers with interlayer space filled by La^{3+} cations. Although Ag_2CdSiS_4 and $BaAg_2SiS_4$ were reported before, related studies on systematic structure regulation and IR NLO property are still absent.[45,46] Structure analysis revealed the fundamental reasons of the tetrahedral framework transformation: the size effect of cations and the reduction of the component tetrahedra caused by cationic substitution change the assembly mode of basic tetrahedral units. Furthermore, Ag_2CdSiS_4, $BaAg_2SiS_4$ and $LaAgSiS_4$ crystals exhibit wide transmittance range (0.5–17 μm), relatively high laser-induced damage thresholds (2 times that of AGS) and significant phase matchable SHG response enhancement (0.6, 1.4 and 3.2 times of AGS). Our work proves that multi-step cation substitution is an effective method to explore potential IR NLO crystals.

Results and discussion

Phase analysis

Single crystals of Ag_2CdSiS_4, $BaAg_2SiS_4$ and $LaAgSiS_4$ were obtained through high-temperature solid state reactions under vacuum (ESI, Fig. S1†). Due to the deviations in the exposure of the sample's crystal planes from the ideal ones, even though the experimental and theoretical powder X-ray diffraction patterns may not look very similar, their purities are still confirmed by the same characteristic peak positions (Fig. S2†). The molar ratios of Ag : M : Si : S obtained by energy-dispersive X-ray spectroscopy are 2.1 : 1 : 1 : 4, 1 : 2.1 : 1.1 : 3.9 and 1 : 1.1 : 1.1 : 4.1 for Ag_2CdSiS_4, $BaAg_2SiS_4$ and $LaAgSiS_4$, respectively, which are in good agreement with those determined from crystal structure analyses (Fig. S3†).

Crystal structures

Similar to AGS, $AgCdSiS_4$ features a three-dimensional diamond-like crystal structure that is close-packed by the vertex-shared AgS_4, CdS_4 and SiS_4 tetrahedra (Fig. 1a and b). Ag_2CdSiS_4 crystalizes in the orthorhombic polar space group $Pmn2_1$ (no. 31) (Table S1†). Its asymmetric unit consists of one Ag (4b), one Cd (2a), one Si (2a) and 3 S atoms occupying two 2a and one 4b sites (Table S2†). However, when two Ga^{3+} cations were replaced by one Cd^{2+} and one Si^{4+}, the AgS_4, CdS_4 and SiS_4 tetrahedra in Ag_2CdSiS_4 exhibits obvious distortion due to the mismatch of geometric sizes, which is manifested in the bond length elongation of the Ag(1)–S(1)#2 (2.973(5) Å), Cd(1)–S(2)#6 (2.929(8) Å) and Si(1)–S(3)#7 (2.456(8) Å) (Table S3†). This case indicates that substitution between different component tetrahedra only change their arrangements and distortions but the diamond-like tetrahedral framework is retained.

To induce structural transformation, the Cd^{2+} ions in Ag_2CdSiS_4 were replaced by larger Ba^{2+} cations. $BaAg_2SiS_4$ crystallize in the tetragonal space group $I\bar{4}2m$ (Table S1†), and its asymmetric unit contains one Ba (2a), one Ag (4d), one Si(2b), and one S (8i) atom. As shown in Fig. 1b, the Ba^{2+} ion is eight-coordinated by surrounding atoms in a distorted bicapped trigonal prismatic geometry, with Ba–S bond lengths ranging from 3.236(12) to 3.301(13) Å. Both Ag and Si are tetrahedrally coordinated by S atoms with Ag–S distance of 2.5997(11) Å and Si–S distance of 2.1245(3) Å (Table S3†). The vertex-sharing interconnection of AgS_4 and SiS_4 tetrahedra result in a three-dimensional open anionic framework with 1D tunnels of 4-member rings, which are filled by charge-balance Ba^{2+} cations (Fig. 1c).

In order to further reduce the dimensionality of the tetrahedral anionic framework, the La^{3+} with higher valence was chosen to simultaneously substitute one Ba^{2+} and one Ag^+ in $BaAg_2SiS_4$. $LaAgSiS_4$ crystallizes in the orthorhombic polar space group *Ama*2 (no. 40). The asymmetric unit of $LaAgSiS_4$ contains one La (4a), one Ag (4b) and three S (4b and 8c) atoms. The La^{3+} cation is eight-coordinated by surrounding S atoms in a LaS_8 bicapped trigonal prism geometry, with the La–S distances varying from 2.924(3) to 3.089(4) Å. Both Ag and Si are tetrahedrally coordinated by S atoms with Ag–S and Si–S distances in the range of 2.495(5)–2.727(4) and 2.117(5)–2.147(7) Å, respectively (Table S3†). When Ba^{2+} was substituted by La^{3+} with higher positive charge, one half of Ag^+ in the anionic framework was eliminated. This led to a change in the connection mode between neighboring tetrahedral groups to sharing both the edge and corner, producing two-dimensional $[AgSiS_4]^{3-}$ layers. These anionic $[AgSiS_4]^{3-}$ layers are packed in an ABAB... pattern along the *a*-axis and separated by the La^{3+} cations (Fig. 1d).

 This journal is © the Partner Organisations 2024

Open Access Article. Published on 29 2024. Downloaded on 2025/11/30 15:27:48.
This article is licensed under a Creative Commons Attribution-NonCommercial 3.0 Unported Licence.

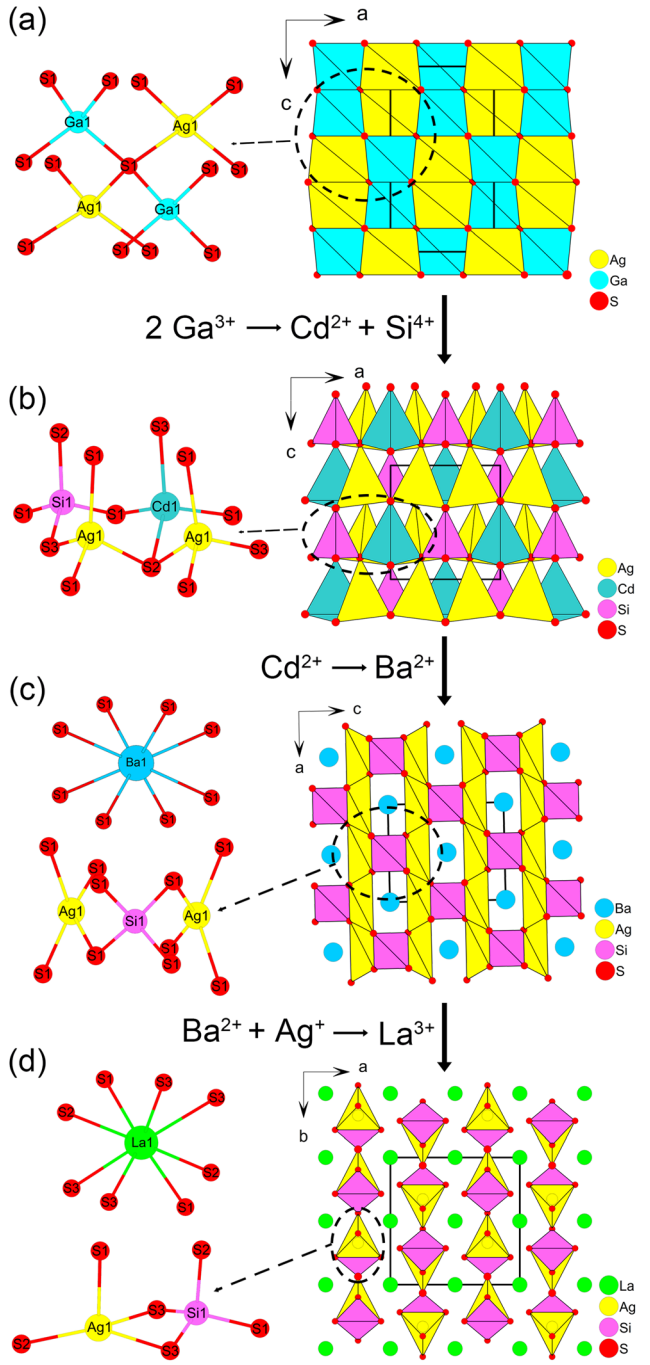

Fig. 1 Vertex-shared AgS_4, GaS_4 tetrahedra; three-dimensional diamond-like $AgGaS_2$ crystal structures (a); vertex-shared AgS_4, CdS_4 and SiS_4 tetrahedra; three-dimensional tetrahedra closed-packed $AgCdSiS_4$ crystal structures (b); coordination environment of Ba^{2+}; vertex-shared AgS_4 and SiS_4 tetrahedra; three-dimensional tunnel structure of $BaAg_2SiS_4$ (c); coordination environment of La^{3+}; edge-shared AgS_4 and SiS_4 tetrahedra; crystal structure of $LaAgSiS_4$ composed of $[AgSiS4]^{3-}$ layers (d).

Cation substitution-induced tetrahedral framework transformation

The crystal structure evolution of three compounds reveals that stepwise cationic substitution from a diamond-like structure is an effective way to extend new structures. To explore the underlying mechanisms, the minimal repeating unit of tetrahedral frameworks was analyzed. As shown in Fig. 1, from Ag_2CdSiS_4 to $BaAg_2SiS_4$ then to $LaAgSiS_4$, accompanied with stepwise substitutions of higher valence cations, the component CdS_4 and AgS_4 tetrahedra in the minimal repeating unit of the tetrahedral frameworks are correspondingly reduced. This reduction of the component tetrahedra not only changes the connection mode of the tetrahedra but also the packing fashion to achieve the corresponding overall frameworks. On the other hand, the larger sizes of Ba^{2+} and La^{3+} cations also aid the formation of tunnels and layers in the tetrahedral frameworks, according to the theory of dimensional reduction.[47] Therefore, the size effect of cations and the reduction of component tetrahedra caused by cation substitutions are the fundamental reasons why the tetrahedral frameworks of three Ag-based quaternary thiosilicates transform from a three-dimensional close-packed structure to a tunneling structure and finally to a two-dimensional layer. In fact, the above analysis also coincides Mei *et al.*'s review on the tetrahedron-based infrared nonlinear materials that the tetrahedral arrangement pattern will evolve with the ratio of metal to tetrahedra.[41]

Optical properties

As shown in the infrared spectrum, the powder samples of all the three compounds exhibit good light transmission in the 2.5–17 μm band, which indicate that the asymmetric Ag_2CdSiS_4, $BaAg_2SiS_4$ and $LaAgSiS_4$ could be potential infrared nonlinear optical materials. The absorption band near 500 cm^{-1} is attributed to the Si–S bond vibration, and the splitting vibration modes may be caused by the SiS_4 tetrahedral distortion (Fig. 2b and S4†).

According to the UV–vis–NIR diffuse reflectance spectrum (Fig. 2a and S5†), the experimental band gap values of Ag_2CdSiS_4, $BaAg_2SiS_4$ and $LaAgSiS_4$ were measured to be 2.56, 2.32, and 2.62 eV, respectively, which are similar to that of AGS (2.72 eV) and match their yellow crystal colors. The unexpected smaller band gap value of $BaAg_2SiS_4$ agree with the reported one, which can be attributed to the outer 5d orbital of Ba^{2+}.[46] Combining the IR spectrum, the title compounds exhibit wide transmittance range from 0.5 to 17 μm.

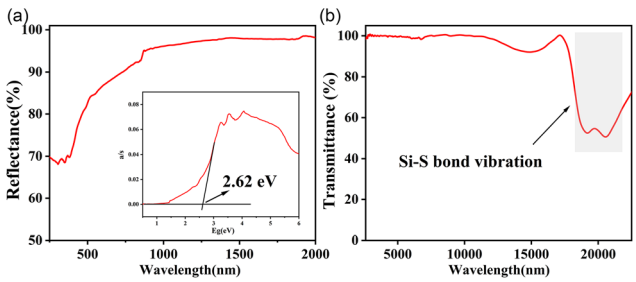

Fig. 2 UV-vis-IR diffuse reflectance spectrum (a) and Fourier transform infrared spectrum (b) of $LaAgSiS_4$.

Open Access Article. Published on 29 2024. Downloaded on 2025/11/30 15:27:48.
This article is licensed under a Creative Commons Attribution-NonCommercial 3.0 Unported Licence.

Particle size-dependent SHG response measurements revealed that three asymmetric Ag_2CdSiS_4, $BaAg_2SiS_4$ and $LaAgSiS_4$ crystals exhibit phase-matchable SHG response intensity of 0.6, 1.4 and 3.2 times that of AGS under 2.05 μm laser irradiation (Fig. 3a and b). By comparing the SHG effect of new and reported thiosilicates, it can be found that $LaAgSiS_4$ achieves the largest SHG effect among known thiosilicates (Fig. 3c).[48–57] Moreover, the SHG effect of title compounds are also comparable to similar thiogeranates and thiogstannates, such as Li_2CdGeS_4 (1 × AGSe), $BaAg_2GeS_4$ (1.7 × AGS), $BaAg_2SnS_4$ (0.4 × AGS), and $BaCdSnS_4$ (0.7 × AGS).[58–65]

Interestingly, from Ag_2CdSiS_4 to $LaAgSiS_4$, their SHG responses increase with the reducing dimensionality of the tetrahedral frameworks. In order to understand the origin of the large SHG difference between polar structural Ag_2CdSiS_4 and $LaAgSiS_4$, their local dipole moments of each fundamental group and unit cell were calculated based on the atomic coordinates. As listed in Table S4,† although the local dipole moments of SiS_4 and AgS_4 tetrahedral groups in both compounds are very close, the net dipole moments of per unit cell in $LaAgSiS_4$ (54.060 D) are much larger than that of Ag_2CdSiS_4 (18.028 D). This indicates that after the introduction of cations, the crystal structures achieve a more ordered arrangement of active groups in $LaAgSiS_4$, which is conducive to the superposition of strong microscopic SHG responses.

The LIDT tests were performed on the single crystals in the 150–210 μm particle size range with AGS as the reference. The results show that the LIDTs of Ag_2CdSiS_4, $BaAg_2SiS_4$ and $LaAgSiS_4$ are about twice of that of AGS (Table S5†), which may be attributed to the stronger Si–S covalent bonds compared with Ga–S bonds and the introduction of strong Ba–S or La–S ionic bonds. In conclusion, Ag_2CdSiS_4, $BaAg_2SiS_4$ and $LaAgSiS_4$ achieve excellent IR NLO properties including large phase matchable SHG effect, wide IR transparent range and high LIDT.

Theoretical calculations

To further understand the relationship between the structures and properties of the title compounds, first-principles calculations based on DFT methods were performed.[66,67] The theoretical band gap values of Ag_2CdSiS_4, $BaAg2SiS_4$, and $LaAgSiS_4$ were calculated to be 1.13, 0.90, 1.57, respectively, which are much smaller compared to the experimental values due to the limitations of the GGA method (Fig. 4a and S6†).

The partial density of states (DOS) analysis revealed the band gap contributions of title compounds (Fig. 4b and S7†). For all the Ag_2CdSiS_4, $BaAg_2SiS_4$ and $LaAgSiS_4$ compounds, the Ag 4d and S 3p orbitals dominated the topmost valence bands (VB). The bottom of the conduction bands (CB), however, are not only contributed by the empty Ag-5s, 5p and unoccupied S-3p orbitals but also dominated by the outer 5d empty orbitals of the heavy cations. Overall, the band gaps of the three compounds are mainly determined by the AgS_4 group, which explains why they exhibit similar direct band gap values.

The theoretical birefringence values (Δn) of Ag_2CdSiS_4, $BaAg_2SiS_4$ and $LaAgSiS_4$ were calculated to be 0.070, 0.169 and 0.080, respectively (Fig. S8†). The suitable Δn of three asymmetric compounds coincide their phase-matching abilities. Given that all three crystal structural frameworks are composed of AgS_4 and SiS_4 tetrahedra, the apparent difference in Δn can be attributed to different tetrahedral arrangements.

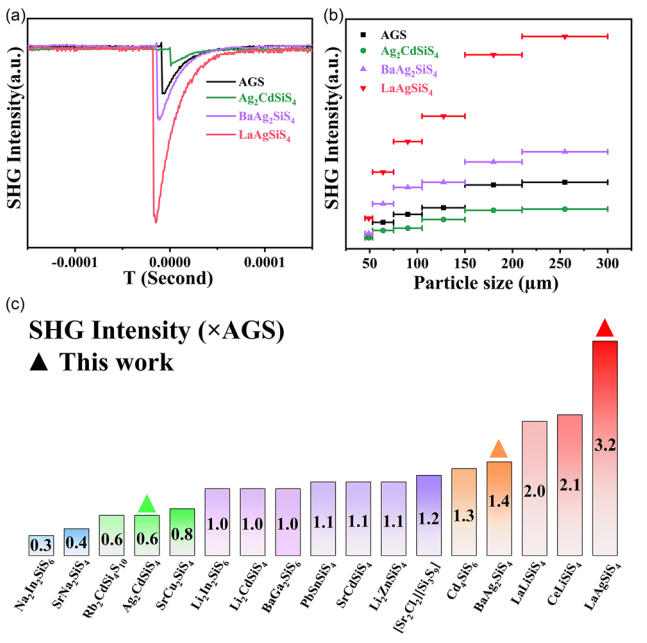

Fig. 3 Particle size-dependent SHG intensity curve for Ag_2CdSiS_4, $BaAg_2SiS_4$ and $LaAgSiS_4$ (a and b); SHG intensity near 2 μm for the title and typical reported thiosilicates (c).

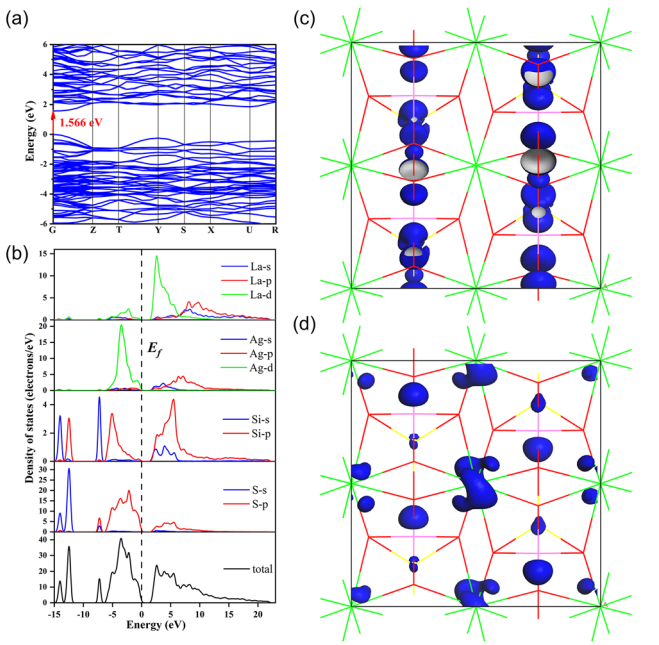

Fig. 4 Calculated band structures (a) and partial density of states (b) and SHG density plots [VB (c) and CB (d)] for $LaAgSiS_4$.

This journal is © the Partner Organisations 2024

Open Access Article. Published on 29 2024. Downloaded on 2025/11/30 15:27:48.
This article is licensed under a Creative Commons Attribution-NonCommercial 3.0 Unported Licence.

Remarkably, the large theoretical birefringence value (Δn) of $BaAg_2SiS_4$ breaks the bias that highly symmetric tetrahedral groups cannot generate large optical anisotropy. Proper crystal structure design is also essential to obtain large optical anisotropy.

The effective NLO coefficients (d_{eff}) of Ag_2CdSiS_4, $BaAg_2SiS_4$ and $LaAgSiS_4$ were calculated to be 7.05, 6.43 and 13.16 pm V^{-1} under the restriction of space group and Kleinman's symmetry, respectively, which agree with the experimental results that $LaAgSiS_4$ achieves a much larger SHG effect. It is worth mentioning that small deviations between experimental and theoretical values may be due to the fact that the experimental samples are powders but the theoretical samples are simulated grown single crystals. The SHG-weighed electron density (SHG density) plots intuitively display the distribution of the source of SHG effects in their crystal structure. As shown in Fig. 4c, d and S9,† in the valence band, the SHG effects originate from the Ag 4d electronic states and S 3p non-bonding states for all three compounds, while in the conduction band, the SHG process is contributed by the unoccupied Ag 5s, Si 3p, and S 3p electronic states for Ag_2CdSiS_4 and $BaAg_2SiS_4$ and by the unoccupied La 5d, Ag 5s, and Si 3p electronic states for $LaAgSiS_4$. The different origins of the SHG effect also explain why they exhibit a large difference in the SHG performance. Furthermore, the contribution percentages of each structure building group were obtained by integrating the SHG density over VB and CB, which turns out to be 34.33%, 44.72% and 20.95% for SiS_4, AgS_4 and CdS_4 groups in Ag_2CdSiS_4; 46.04%, 44.96% and 9.00% for SiS_4, AgS_4 and Ba^{2+} in $BaAg_2SiS_4$; 32.88%, 26.25% and 40.87% for SiS_4, AgS_4 and LaS_8 groups in $LaAgSiS_4$, respectively. For Ag_2CdSiS_4 and $BaAg_2SiS_4$, the tetrahedral group dominates the SHG contribution, while for $LaAgSiS_4$, the LaS_8 group contributes more, which emphasizes the benefits of adopting multi-step cation substitution to introduce well-performing functional crystal material genes.

Conclusions

In summary, three quaternary thiosilicates, namely, Ag_2CdSiS_4, $BaAg_2SiS_4$ and $LaAgSiS_4$, were designed and synthesized successfully through multi-step cation substitutions from AGS. Interestingly, their tetrahedral frameworks transform from a three-dimensional close-packed structure to a tunneling structure and finally to a two-dimensional layered structure, which was essentially caused by the size effect of cations and the cation substitution-induced component tetrahedra reduction. In addition, as IR NLO materials, Ag_2CdSiS_4, $BaAg_2SiS_4$ and $LaAgSiS_4$ crystals exhibit wide transmittance range (0.5–17 μm), relatively high laser-induced damage thresholds (2 times that of AGS), phase-matching ablility, and significant SHG response enhancement (0.6, 1.4 and 3.2 times of AGS, respectively), which results from the more ordered arrangement of active groups induced by cationic substitution. Theoretical calculations suggest that the large SHG effects of $LaAgSiS_4$ originated from not only SiS_4 and AgS_4 tetrahedral groups but also from the active LaS_8 cationic genes introduced through multi-step cation substitution. This work demonstrates the multi-step substitution-induced crystal structure transformation and nonlinear optical performance enhancement, indicating that multi-step cation substitution is an effective method to explore potential functional IR NLO crystal materials.

Data availability

Supporting data for this article is presented in the ESI.† The raw data of this article can be obtained by contacting the corresponding author.

Conflicts of interest

There are no conflicts to declare.

Acknowledgements

The authors thank Dr Bing-Xuan Li (Fujian Institute of Research on Structure of Matter, Chinese Academy of Sciences) for his help with the LIDT tests. This work was supported by the National Natural Science Foundation of China (No. 22031009, 22375201 and 21921001).

References

1 Y. Tang, K. Li, X. Zhang, J. Deng, G. Li and E. Brasselet, Harmonic spin-orbit angular momentum cascade in nonlinear optical crystals, *Nat. Photonics*, 2020, **14**, 658–662.
2 T. Verbiest, S. V. Elshocht, M. Kauranen, L. Hellemans, J. Snauwaert, C. Nuckolls, T. J. Katz and A. Persoons, Strong enhancement of nonlinear optical properties through supramolecular chirality, *Science*, 1998, **282**, 913–915.
3 F. Capasso, R. Paiella, R. Martini, R. Colombelli, C. Gmachl, T. L. Myers, M. S. Taubman, R. M. Williams, C. G. Bethea, K. Unterrainer, H. Y. Hwang, D. L. Sivco, A. Y. Cho, A. M. Sergent, H. C. Liu and E. A. Whittaker, Quantum cascade lasers: ultrahigh-speed operation, optical wireless communication, narrow linewidth, and far-infrared emission, *IEEE J. Quantum Electron.*, 2002, **38**, 511–532.
4 D. F. Eaton, Nonlinear optical materials, *Science*, 1991, **253**, 281–287.
5 S. Guo, Y. Chi and G. Guo, Recent achievements on middle and far-infrared second-order nonlinear optical materials, *Coord. Chem. Rev.*, 2017, **335**, 44–57.
6 G. C. Catella, L. R. Shiozawa, J. R. Hietanen, R. C. Eckardt, R. K. Route, R. S. Feigelson, D. G. Cooper and C. L. Marquardt, Mid-IR absorption in aggase2 optical parametric oscillator crystals, *Appl. Opt.*, 1993, **32**, 3948–3951.

Open Access Article. Published on 29 2024. Downloaded on 2025/11/30 15:27:48. This article is licensed under a Creative Commons Attribution-NonCommercial 3.0 Unported Licence.

7 A. Harasaki and K. Kato, New Data on the nonlinear optical constant, phase-matching, and optical damage of $AgGaS_2$, *Jpn. J. Appl. Phys.*, 1997, **36**, 700–703.
8 P. A. Budni, L. A. Pomeranz, M. L. Lemons, C. A. Miller, J. R. Mosto and E. P. Chicklis, Efficient mid-infrared laser using 1.9 μm-pumped Ho:YAG and $ZnGeP_2$ optical parametric oscillators, *J. Opt. Soc. Am. B*, 2000, **17**, 723–728.
9 K. Wu and S. Pan, A review on structure-performance relationship toward the optimal design of infrared nonlinear optical materials with balanced performances, *Coord. Chem. Rev.*, 2018, **377**, 191–208.
10 F. Liang, L. Kang, Z. Lin and Y. Wu, Mid-infrared nonlinear optical materials based on metal chalcogenides: structure–property relationship, *Cryst. Growth Des.*, 2017, **17**, 2254–2289.
11 F. Hou, D. Mei, M. Xia and Y. Wu, Structure-performance relationship in tri-coordinated nonlinear optical materials toward optimal second harmonic generation and phase matching, *Coord. Chem. Rev.*, 2021, **444**, 214038.
12 Y. Li, J. Luo and S. Zhao, Local polarity-induced assembly of second-order nonlinear optical materials, *Acc. Chem. Res.*, 2022, **55**, 3460–3469.
13 J. H. Feng, C. L. Hu, X. Xu, B. X. Li, M. J. Zhang and J. G. Mao, $AgGa_2PS_6$: A New Mid–Infrared Nonlinear Optical Material with a High Laser Damage Threshold and a Large Second Harmonic Generation Response, *Chem. – Eur. J.*, 2017, **23**, 10978–10982.
14 W. Xing, F. Liang, C. Tang, E. Uykur, Z. Lin, J. Yao, W. Yin and B. Kang, Highly Distorted $[HgS_4]$ Motif-Driven Structural Symmetry Degradation and Strengthened Second-Harmonic Generation Response in the Defect Diamond-Like Chalcogenide $Hg_3P_2S_8$, *ACS Appl. Mater. Interfaces*, 2021, **13**, 37331–37338.
15 A. Abudurusuli, J. Huang, P. Wang, Z. Yang, S. Pan and J. Li, $Li_4MgGe_2S_7$: The First Alkali and Alkaline-Earth Diamond-Like Infrared Nonlinear Optical Material with Exceptional Large Band Gap, *Angew. Chem., Int. Ed.*, 2021, **60**, 24131–24136.
16 B. Tell and H. M. Kasper, Optical and Electrical Properties of $AgGaS_2$ and $AgGaSe_2$, *Phys. Rev. B*, 1971, **4**, 4455–4459.
17 T. K. Bera, J. H. Song, A. J. Freeman, J. I. Jang, J. B. Ketterson and M. G. Kanatzidis, Soluble direct-band-gap semiconductors $LiAsS_2$ and $NaAsS_2$: large electronic structure effects from weak AS...S interactions and strong nonlinear optical response, *Angew. Chem., Int. Ed.*, 2008, **47**, 7828–7832.
18 M. C. Chen, L. M. Wu, H. Lin, L. J. Zhou and L. Chen, sconnection enhances the second harmonic generation response: synthesis and characterization of $Ba_{23}Ga_8Sb_2S_{38}$, *J. Am. Chem. Soc.*, 2012, **134**, 6058–6060.
19 Y. X. Han, C. L. Hu, Z. Fang, Q. Q. Chen, B. X. Li, Y. Lin and J. G. Mao, a promising mid-infrared nonlinear optical material, *J. Mater. Chem. C*, 2022, **10**, 12556–12559.
20 C. Li, W. Yin, P. Gong, X. Li, M. Zhou, A. Mar, Z. Lin, J. Yao, Y. Wu and C. Chen, Trigonal planar $[HgSe_3]^{4-}$ unit: a new kind of basic functionalgroup in ir nonlinear optical materials with large susceptibility and physicochemical stability, *J. Am. Chem. Soc.*, 2016, **138**, 6135–6138.
21 B. W. Liu, X. M. Jiang, H. Y. Zeng and G. C. Guo, Li $[LiCs_2Cl][Ga_3S_6]$: Unprecedented Tetrahedra-built Nanoporous Framework with Excellent Nonlinear Optical Performance, *J. Am. Chem. Soc.*, 2020, **142**, 10641–10645.
22 Y. Zhang, H. Wu, Z. Hu, J. Wang, Y. Wu and H. Yu, Achieving a strong second harmonic generation response and a wide band gap in a Hg-based material, *Inorg. Chem. Front.*, 2022, **9**, 4075–4080.
23 H. Chen, W. B. Wei, H. Lin and X. T. Wu, Transition-metal-based chalcogenides: A rich source of infrared nonlinear optical materials, *Coord. Chem. Rev.*, 2021, **448**, 214154.
24 X. Lin, G. Zhang and N. Ye, Growth and Characterization of $BaGa4S_7$: A New Crystal for Mid-IR Nonlinear Optics, *Cryst. Growth Des.*, 2009, **9**, 1186–1189.
25 J. Yao, D. Mei, L. Bai, Z. Lin, W. Yin, P. Fu and Y. Wu, BaGa4Se7: A New Congruent-Melting IR Nonlinear Optical Material, *Inorg. Chem.*, 2010, **49**, 9212–9216.
26 J. Chen, C. Lin, S. Yang, X. Jiang, S. Shi, Y. Sun, B. Li, S. Fang and N. Ye, Cd_4SiQ_6 (Q = S, Se): Ternary Infrared Nonlinear Optical Materials with Mixed Functional Building Motifs, *Cryst. Growth Des.*, 2020, **20**, 2489–2496.
27 S. Lee, S. L. Carnahan, G. Akopov, P. Yox, L. L. Wang, A. J. Rossini, K. Wu and K. Kovnir, Noncentrosymmetric Tetrel Pnictides $RuSi4P_4$ and $IrSi3P_3$: Nonlinear Optical Materials with Outstanding Laser Damage Threshold, *Adv. Funct. Mater.*, 2021, **31**, 2010293.
28 H. Zhang, M. Zhang, S. Pan, X. Dong, Z. Yang, X. Hou, Z. Wang, K. B. Chang and K. R. Poeppelmeier, $Pb_{17}O_8Cl_{18}$: A Promising IR Nonlinear Optical Material with Large Laser Damage Threshold Synthesized in an Open System, *J. Am. Chem. Soc.*, 2015, **137**, 8360–8363.
29 X. Chen, H. Jo and K. M. Ok, Lead Mixed Oxyhalides Satisfying All Fundamental Requirements for High-Performance Mid-Infrared Nonlinear Optical Materials, *Angew. Chem., Int. Ed.*, 2020, **59**, 7514–7520.
30 S. Yang, C. Lin, H. Fan, K. Chen, G. Zhang, N. Ye and M. Luo, Polar Phosphorus Chalcogenide Cage Molecules: Enhancement of Nonlinear Optical Properties in Adducts, *Angew. Chem., Int. Ed.*, 2023, **62**, e202218272.
31 J. Chen, C. Lin, D. Zhao, M. Luo, G. Peng, B. Li, S. Yang, Y. Sun and N. Ye, Anionic Aliovalent Substitution from Structure Models of ZnS: Novel Defect Diamond-like Halopnictide Infrared Nonlinear Optical Materials with Wide Band Gaps and Large SHG Effects, *Angew. Chem., Int. Ed.*, 2020, **59**, 23549–23553.
32 W. Zhou, J. Wu, W. Liu and S.-P. Guo, Ag-based chalcogenides and derivatives as promising infrared nonlinear optical materials, *Coord. Chem. Rev.*, 2023, **477**, 214950.
33 L. Kang, M. Zhou, J. Yao, Z. Lin, Y. Wu and C. Chen, Metal Thiophosphates with Good Mid-infrared Nonlinear Optical Performances: A First-Principles Prediction and Analysis, *J. Am. Chem. Soc.*, 2015, **137**, 13049–13059.
34 Z. Yang and S. Pan, Computationally assisted multistage design and prediction driving the discovery of deep-ultra-

 This journal is © the Partner Organisations 2024

Open Access Article. Published on 29 2024. Downloaded on 2025/11/30 15:27:48.
This article is licensed under a Creative Commons Attribution-NonCommercial 3.0 Unported Licence.

violet nonlinear optical materials, *Mater. Chem. Front.*, 2021, **5**, 3507–3523.

35 C. L. Hu, Y. X. Han, Z. Fang and J. G. Mao, Zn_2BS_3Br: An Infrared Nonlinear Optical Material with Significant Dual-Property Enhancements Designed through a Template Grafting Strategy, *Chem. Mater.*, 2023, **35**, 2647–2654.

36 W. Cai, A. Abudurusuli, C. Xie, E. Tikhonov, J. Li, S. Pan and Z. Yang, Toward the Rational Design of Mid-Infrared Nonlinear Optical Materials with Targeted Properties via a Multi-Level Data-Driven Approach, *Adv. Funct. Mater.*, 2022, **32**, 2200231.

37 M. L. Liang, C. L. Hu, F. Kong and J. G. Mao, $BiFSeO_3$: An Excellent SHG Material Designed by Aliovalent Substitution, *J. Am. Chem. Soc.*, 2016, **138**, 9433–9436.

38 H. Lin, W.-B. Wei, H. Chen, X. T. Wu and Q. L. Zhu, Rational design of infrared nonlinear optical chalcogenides by chemical substitution, *Coord. Chem. Rev.*, 2020, **406**, 213150.

39 J. Chen, C. L. Hu, F. Kong and J. G. Mao, High-Performance Second-Harmonic-Generation (SHG) Materials: New Developments and New Strategies, *Acc. Chem. Res.*, 2021, **54**, 2775–2783.

40 Q. Q. Liu, X. Liu, L. M. Wu and L. Chen, $SrZnGeS_4$: A Dual-Waveband Nonlinear Optical Material with a Transparency Spanning UV/Vis and Far-IR Spectral Regions, *Angew. Chem., Int. Ed.*, 2022, **61**, e202205587.

41 W. Wang, D. Mei, F. Liang, J. Zhao, Y. Wu and Z. Lin, Inherent laws between tetrahedral arrangement pattern and optical performance in tetrahedron-based mid-infrared nonlinear optical materials, *Coord. Chem. Rev.*, 2020, **421**, 213444.

42 J. Chen, H. Chen, F. Xu, L. Cao, X. Jiang, S. Yang, Y. Sun, X. Zhao, C. Lin and N. Ye, $Mg_2In_3Si_2P_7$: A Quaternary Diamond-like Phosphide Infrared Nonlinear Optical Material Derived from $ZnGeP_2$, *J. Am. Chem. Soc.*, 2021, **143**, 10309–10316.

43 B. W. Liu, X. M. Jiang, B. X. Li, H. Y. Zeng and G. C. Guo, Li $[LiCs_2Cl][Ga_3S_6]$: A Nanoporous Framework of GaS_4 Tetrahedra with Excellent Nonlinear Optical Performance, *Angew. Chem., Int. Ed.*, 2020, **59**, 4856–4859.

44 F. Liang, L. Kang, Z. Lin, Y. Wu and C. Chen, Mid-Infrared Nonlinear Optical Materials Based on Metal Chalcogenides: Structure–Property Relationship, *Coord. Chem. Rev.*, 2017, **333**, 57–70.

45 O. V. Parasyuk and L. V. Piskach, Phase Equilibria in the Ag_2SiS_3-CdS System, *Russ. J. Inorg. Chem.*, 1999, **44**, 970–971.

46 J.-P. Sun, G. C. McKeown Wessler, T. Wang, T. Zhu, V. Blum and D. B. Mitzi, Structural Tolerance Factor Approach to Defect-Resistant I_2-II-IV-X_4 Semiconductor Design, *Chem. Mater.*, 2020, **32**, 1636–1649.

47 E. G. Tulsky and J. R. Long, Dimensional Reduction: A Practical Formalism for Manipulating Solid Structures, *Chem. Mater.*, 2001, **13**, 1149–1166.

48 Y. Yang, K. Wu, X. Wu, B. Zhang and L. Gao, A new family of quaternary thiosilicates SrA_2SiS_4 (A = Li, Na, Cu) as promising infrared nonlinear optical crystals, *J. Mater. Chem. C*, 2020, **8**, 1762–1767.

49 J. Zhou, Z. Fan, K. Zhang, Z. Yang, S. Pan and J. Li, $Rb_2CdSi_4S_{10}$: novel $[Si_4S_{10}]$ T2-supertetrahedra-contained infrared nonlinear optical material with large band gap, *Mater. Horiz.*, 2023, **10**, 619–624.

50 W. Yin, K. Feng, W. Hao, J. Yao and Y. Wu, Synthesis, Structure, and Properties of $Li_2In_2MQ_6$ (M = Si, Ge. Q = S, Se): A New Series of IR Nonlinear Optical Materials, *Inorg. Chem.*, 2012, **51**, 5839–5843.

51 G. M. Li, Y. Chu, J. Li and Z. X. Zhou, Li_2CdSiS_4, a promising IR NLO material with a balanced Eg and SHG response originating from the effect of Cd with d^{10} configuration, *Dalton Trans.*, 2020, **49**, 1975–1980.

52 G. Li, Y. Chu and Z. Zhou, From $AgGaS_2$ to Li_2ZnSiS_4: Realizing Impressive High Laser Damage Threshold Together with Large Second-Harmonic Generation Response, *Chem. Mater.*, 2018, **30**, 602–606.

53 B. W. Liu, H. Y. Zeng, M. J. Zhang, Y. H. Fan, G. C. Guo, J. S. Huang and Z. C. Dong, Syntheses, Structures, and Nonlinear-Optical Properties of Metal Sulfides $Ba_2Ga_8MS_{16}$ (M = Si, Ge), *Inorg. Chem.*, 2015, **54**, 976–981.

54 J. Zhou, L. Luo, Y. Chu, P. Wang, Z. Guo, X. Su and J. Li, Partial congener substitution induced centrosymmetric to noncentrosymmetric structural transformation and nonlinear optical properties of $PbSnSiS_4$, *J. Alloys Compd.*, 2022, **899**, 163366.

55 H. D. Yang, M. Y. Ran, S. H. Zhou, X. T. Wu, H. Lin and Q. L. Zhu, Rational design via dual-site aliovalent substitution leads to an outstanding IR nonlinear optical material with well-balanced comprehensive properties, *Chem. Sci.*, 2022, **13**, 10725–10733.

56 C. Zhao, K. Wu, Y. Xiao, B. Zhang, H. Yu and H. Zhang, $[Sr_4Cl_2][Si_3S_9]$: Ultrawide-bandgap salt-inclusion thiosilicate nonlinear optical material with unprecedented tri-polymerized $[Si_3S_9]$ clusters, *J. Mater. Chem. C*, 2023, **11**, 4439–4443.

57 Y. X. Han, C. L. Hu, B. X. Li and J. G. Mao, $LnLiSiS_4$ (Ln = La and Ce): Promising infrared nonlinear optical materials designed by aliovalent substitution from $SrCdSiS_4$, *Mater. Today Phys.*, 2023, **31**, 100987.

58 L. Nian, K. Wu, G. He, Z. Yang and S. Pan, Effect of Element Substitution on Structural Transformation and Optical Performances in $I_2BaMIVQ_4$ (I = Li, Na, Cu, and Ag. MIV = Si, Ge, and Sn. Q = S and Se), *Inorg. Chem.*, 2018, **57**, 3434–3442.

59 J. A. Brant, D. J. Clark, Y. S. Kim, J. I. Jang, J. Zhang and J. A. Aitken, Li_2CdGeS_4, A Diamond-Like Semiconductor with Strong Second-Order Optical Nonlinearity in the Infrared and Exceptional Laser Damage Threshold, *Chem. Mater.*, 2014, **26**, 3045–3048.

60 H. Chen, P. Liu, B. Li, H. Lin, L. Wu and X. Wu, Experimental and theoretical studies on the NLO properties of two quaternary non-centrosymmetric chalcogenides: $BaAg_2GeS_4$ and $BaAg_2SnS_4$, *Dalton Trans.*, 2018, **47**, 429–437.

Open Access Article. Published on 29 2024. Downloaded on 2025/11/30 15:27:48.
This article is licensed under a Creative Commons Attribution-NonCommercial 3.0 Unported Licence.

61 Y. Guo, F. Liang, W. Yin, Z. Li, X. Luo, Z. Lin, J. Yao, A. Mar and Y. Wu, $BaHgGeSe_4$ and $SrHgGeSe_4$: Two New Hg-Based Infrared Nonlinear Optical Materials, *Chem. Mater.*, 2019, **31**, 3034–3040.

62 N. Zhen, K. Wu, Y. Wang, Q. Li, W. Gao, D. Hou, Z. Yang, H. Jiang, Y. Dong and S. Pan, $BaCdSnS_4$ and $Ba_3CdSn_2S_8$: syntheses, structures, and non-linear optical and photoluminescence properties, *Dalton Trans.*, 2016, **45**, 10681–10688.

63 W. Zhou, Q. Zhang, W. Yao, H. Xue and S. Guo, Stepwise Li Substitution Induced Structure Evolution and Improved Nonlinear Optical Performance for Diamond-like Sulfides, *Inorg. Chem.*, 2021, **60**, 12536–12544.

64 W. Zhou, W. Liu and S. Guo, $(Na_{0.74}Ag_{1.26})BaSnS_4$: A New $AgGaS_2$-Type Nonlinear Optical Sulfide with a Wide Band Gap and High Laser Induced Damage Threshold, *Chem. – Eur. J.*, 2022, **28**, e202202063.

65 M. Yan, Z. Sun, W. Yao, W. Zhou, W. Liu and S. Guo, A highly distorted HgS_4 tetrahedron-induced moderate second-harmonic generation response of $EuHgGeS_4$, *Inorg. Chem. Front.*, 2020, **7**, 2451–2458.

66 V. Milman, B. Winkler, J. A. White, C. J. Pickard, M. C. Payne, E. V. Akhmatskaya and R. H. Nobes, Electronic structure, properties, and phase stability of inorganic crystals: A pseudopotential plane-wave study, *J. Quantum Chem.*, 2000, **77**, 895–910.

67 M. D. Segall, P. J. D. Lindan, M. J. Probert, C. J. Pickard, P. J. Hasnip, S. J. Clark and M. C. Payne, First-principles simulation: ideas, illustrations and the CASTEP code, *J. Phys.: Condens. Matter*, 2002, **14**, 2717–2744.

 This journal is © the Partner Organisations 2024